Fibers with Integrated Mechanochemical Switches: Minimalistic Design Principles Derived from Fibronectin

Orit Peleg,[†‡] Thierry Savin,[‡] German V. Kolmakov,[§] Isaac G. Salib,[§] Anna C. Balazs,[§] Martin Kröger,[‡*] and Viola Vogel[†*]

[†]Laboratory of Applied Mechanobiology, Department of Health Sciences and Technology and [‡]Polymer Physics, Department of Materials, ETH Zürich, Zürich, Switzerland; and [§]Chemical Engineering Department, University of Pittsburgh, Pittsburgh, Pennsylvania

ABSTRACT Inspired by molecular mechanisms that cells exploit to sense mechanical forces and convert them into biochemical signals, chemists dream of designing mechanochemical switches integrated into materials. Using the adhesion protein fibronectin, whose multiple repeats essentially display distinct molecular recognition motifs, we derived a computational model to explain how minimalistic designs of repeats translate into the mechanical characteristics of their fibrillar assemblies. The hierarchy of repeat-unfolding within fibrils is controlled not only by their relative mechanical stabilities, as found for single molecules, but also by the strength of cryptic interactions between adjacent molecules that become activated by stretching. The force-induced exposure of cryptic sites furthermore regulates the nonlinearity of stress-strain curves, the strain at which such fibers break, and the refolding kinetics and fraction of misfolded repeats. Gaining such computational insights at the mesoscale is important because translating protein-based concepts into novel polymer designs has proven difficult.

INTRODUCTION

Only a few attempts have been made so far to design polymeric materials with integrated mechanochemical switches (1–4). Recently, various structural motifs have been described for intra- and extracellular proteins, explaining how their stretching might switch the display of binding sites that can thus be either activated or destroyed by tensile forces (5–8). So-called cryptic binding sites that become exposed upon mechanical unfolding include phosphorylation sites (9), hydrophobic residues (10), amphipathic helices (11,12), cysteines (13–15), enzymatic cleavage sites (16), and activators of enzymatic activity (17). Alternatively, multidomain binding motifs, which are destroyed by stretching the domain-domain distance, can also exist (18). All of the aforementioned mechanoregulated intra- and extracellular systems can be switched by cell traction forces or by external forces acting on extended force-bearing protein networks in which such switches are embedded.

Assembly into fibrillar networks is common to most extracellular matrix (ECM) proteins, and the multidomain protein fibronectin (Fn) is one of the most extensively studied mechanoregulated ECM proteins (7,19). Fn is a high-molecular-mass (440 kDa) ECM glycoprotein that plays a major role in regulating cell adhesion, migration, and diverse tissue functions, including wound healing and embryonic development (19). Fn is composed of ~ 30 repeats, each 50–100 amino acids long and rich in β-sheet motifs (7). We show a typical Fn repeat in Fig. 1 *a*. Several repeats contain cryptic binding sites, some of which regulate Fn fibrillogenesis (7,8,19,20) and others of which, such as the binding sites for the bacterial adhesins, are destroyed upon stretching (18). Atomistic computational techniques, mainly steered molecular dynamics, played a central role in deciphering the structural events by which single repeats are mechanically unfolded (21,22). In particular, it was revealed that clusters of several force-bearing, backbone hydrogen bonds must break simultaneously to pass the major energy barrier of the conformational switch (7,20). Yet it remains unknown how the design of a multimodular Fn molecule enables its multiple mechanoregulated functions, nor is it understood how its structure also ensures that the Fn fibrils can reversibly relax upon stretching (14,23).

To learn how the design of repeats and their structural arrangement within fibers, and the presence of noncryptic and cryptic Fn-Fn interactions regulate the mesoscopic mechanical characteristics of Fn fibers, novel coarse-grained computational approaches are needed. Deriving minimalistic design features that are simple enough to be converted into the synthetic world would be greatly facilitated by a coarse-grained model that mimics basic yet general features of a mechanoresponsive protein. Previously, coarsening of multimodular proteins was done by defining each module as a single repeat connected to its neighbor by a two-state, double-well bond potential (24–26). Such approaches have significantly extended the size limit to handle large fibers, but are too simplistic to handle cryptic sites without introducing numerical singularities.

Here we present an intermediate mesoscopic model that is able to simulate large systems while keeping track of the essential nanostructural features (Fig. 1). Our approach is specifically designed to capture all of the essential

Submitted July 4, 2012, and accepted for publication September 21, 2012.

*Correspondence: mk@mat.ethz.ch or viola.vogel@hest.ethz.ch

Orit Peleg's present address is Institute of Neuroinformatics, University of Zürich and ETH Zürich, Zürich, Switzerland.

Editor: Gerhard Hummer.

0006-3495/12/11/1909/10 $2.00

http://dx.doi.org/10.1016/j.bpj.2012.09.028

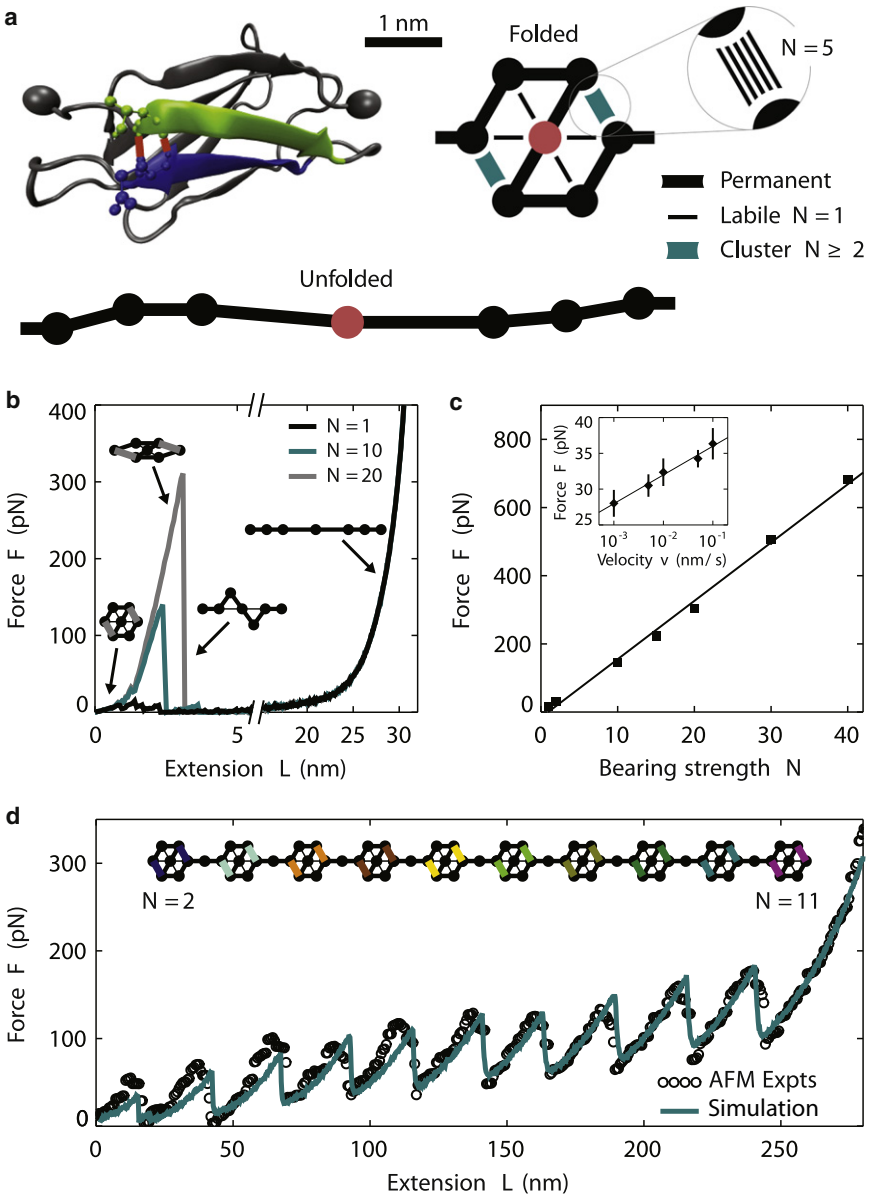

FIGURE 1 Coarse-grained model of native Fn complexes and a single chain. (*a*) Structure of the $FnIII_7$ module (Protein Data Bank entry code 1FNF), in which the force-bearing hydrogen bonds between the green (F) and blue (G) β-strands are shown in red (60), and the C- and N-terminals are marked with black spheres. Our coarse-grained representation consists of six surface sites (*black spheres*) and one cryptic site (*red sphere*) connected by permanent backbone bonds (*thick black lines*) and labile bonds (*thin lines*) and their clusters (color-coded for the value of N as in panel *d*). The unfolded state, obtained when all labile bonds ruptured, exposes the cryptic site. (*b*) Force versus extension at constant velocity for repeats of varying strength N. (*c*) Maximal tensile force before the secondary structure starts to unravel by pulling the repeat across an energy barrier, as a function of the bond strength N. Inset: The activation force of repeat $N = 5$ as a function of the pulling velocity. (*d*) Force versus extension for the model Fn chain, built by linearly connecting 10 repeats of different bearing strengths ($N = 2, \ldots, 11$) as shown in the inset, compared with the experimental (28) force-extension curve of native Fn.

mechanical features of multimodular Fn while permitting a microscopic exploration of the minimal features a simplified system must have to mimic the central properties of mechanoresponsive fibrils. First, the repeat unfolding trajectory under tensile force is characterized by a single dominant force peak that is associated with the breakage of a cluster of bonds. Second, the repeats can reversibly refold when relaxed. Finally, the contour length of the chain is increased when the repeat is opened. To simulate the behavior that is associated with fibrillogenesis (7), the repeat is designed here to expose upon opening a cryptic site that can specifically bind to neighboring chains. In the folded configuration, our bead-spring module is thus composed of seven sites that are hexagonally arranged along a permanent Z-shaped backbone. The latter is maintained by six labile bonds to form a shielding shell around the central cryptic site. The labile bonds are linear springs that are allowed to break and reform (see Materials and Methods section). Four of these are structural bonds (*thin black lines* in Fig. 1 *a*) between the cryptic site and the surrounding shell, and two of them mimic force-bearing clusters of bonds (*colored lines* in Fig. 1 *a*). These two force-bearing bonds are each made of a cluster of N parallel labile bonds that are used to tune the relative mechanical stability of the repeats, a feature typically found in multidomain proteins that have mechanical functions (7,8,22,27–29). N is conveniently the only parameter we vary to control the activation barrier of the otherwise identical model repeats. The methods we used to compute the motion of sites, kinetics of rupture, and rebinding of all labile bonds are described next.

MATERIALS AND METHODS

The repeat's backbone (Fig. 1) is formed by repulsive Lennard-Jones sites that are linearly and permanently connected by two kinds of attractive (either weakly or strongly) finitely extendable nonlinear elastic (FENE (30,31)) springs. The FENE model allows us to adjust the contour length of the repeat in its unfolded conformation. A molecular chain is modeled as a linearly connected sequence of n repeats along the same backbone (see *inset* of Fig. 1 *d*), and a fiber is built as an assembly of m chains held together by interchain interactions (Fig. 2). The FENE force law is given by $F(r) = k(r-a)/(1-[r-a]^2/d^2)$ for bond length $r \geq a$, where d denotes the maximum bond stretch, k is the spring coefficient, and $a = 1.3$nm is a rest length maintained by the repulsive interaction. Both parameters d and k depend on the kind of bond: permanent bonds connecting the cryptic site (Fig. 1) to its neighbors are long and weak, with corresponding parameters $d_w = 10.4$nm and $k_w = 0.9$pN/nm, whereas the rest of the backbone bonds are short and strong, with $d_s = 1.8$nm and $k_s = 220 \times k_w$. The labile bonds (inter- and intrachain interactions) are formed by linear springs, with force law $F(r) = \kappa(r-a)$ (where $\kappa = 17.7$pN/nm), that have a force-dependent breaking and reforming rate (see below).

The motion of the sites is calculated via a simple hybrid Brownian dynamics-Monte Carlo simulation (30). The trajectory follows a conventional overdamped Langevin equation. Thus, the streaming velocity of a site is taken to be proportional to the net force acting on it. The discretized Langevin equation indeed gives the site's velocity $\dot{\mathbf{r}} = \mu\mathbf{F} + \sqrt{2k_BT\mu/\Delta t}\mathbf{W}$, where μ is the mobility, k_B is the Boltzmann constant, T is the temperature, Δt is the time step, $\mathbf{F}$ is the total force acting on the site, and $\mathbf{W}$ is a zero-mean random white noise vector with unit variance. During deformations of chains and fibers, designated chain ends are enforced to move at constant speed v in the direction of extension, while all remaining components remain unconstrained. The kinetics of rupture and rebinding of all labile bonds under load is controlled by the hierarchical Bell model (24,29), which offers an approximate (32,33) relationship between bond dissociation/association rate and force. Accordingly, the state of the labile bonds is tested stochastically at each time step.

We set the values of model parameters such that the mechanical behaviors of native FnIII segments and their chains are reproduced (Fig. 1 *d*). Notably, we also ensure that the isolated repeat is stable in its folded configuration. Further implementation details and a complete list of simulation parameters and their values are given in the Supporting Material.

RESULTS AND DISCUSSION

Single repeats

We first assess the mechanical response of a single repeat under tensile deformation by moving the terminal ends apart with a constant velocity v (*insets* of Fig. 1 *b*). With increasing deformation, the pulling force increases almost linearly with the extension until the two force-bearing clusters of N labile bonds break almost simultaneously, giving rise to a single peak, which we will call the activation peak, in the force-extension response curve (Fig. 1 *b*). After

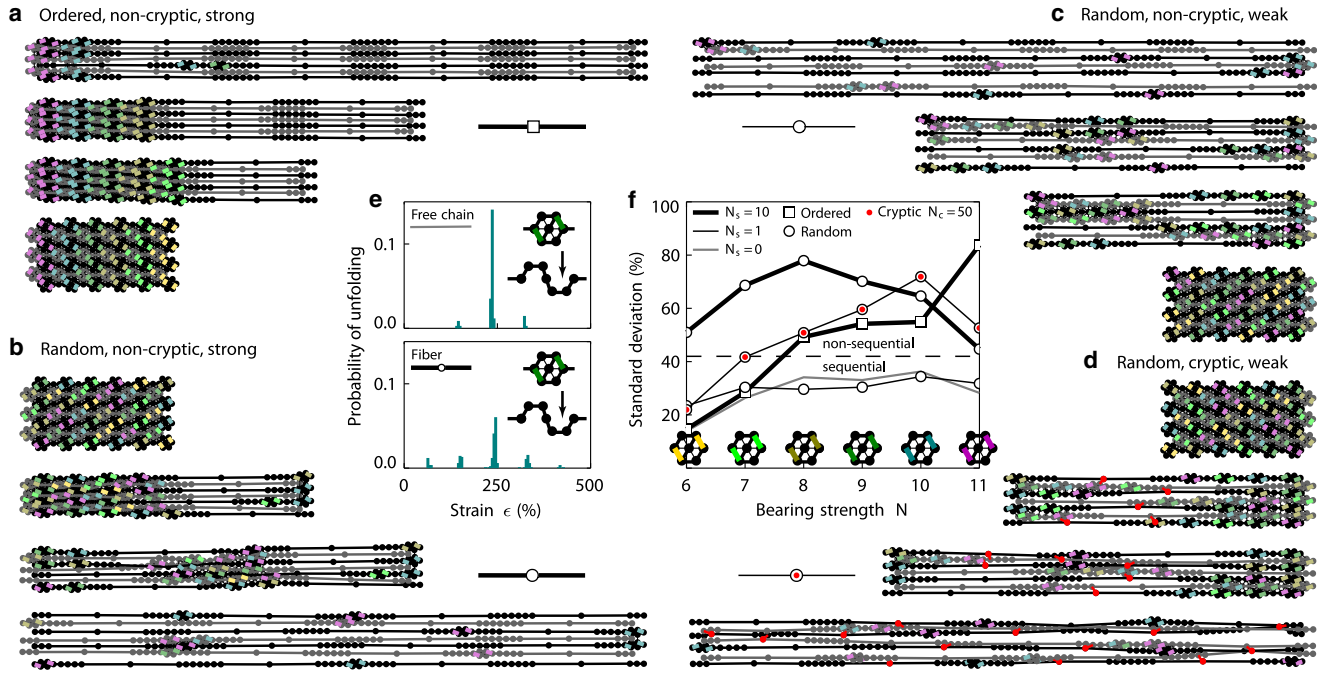

FIGURE 2 Repeat unfolding statistics for various designs of fiber models built with $m = 7$ chains of $n = 6$ repeats with $N_{max} = 11$. (*a*) Snapshots of the extended fiber made of ordered chains without cryptic sites but moderate surface interchain interactions, $N_s = 10 \approx N_{max}$. (*b*) The same as panel *a* but with a random fiber. (*c*) Extensional test for a random fiber with weak surface bonds ($N_s = 1$) and without cryptic sites. (*d*) The same as panel *c* but with strong cryptic interchain bonds composed of $N_c = 50 \gg N_{max}$. Fully animated sequences for *a–d* are shown in Movie S1. (*e*) Probability distribution of unfolding the repeat $N = 8$ as a function of the strain during the extension test. The top graph is for an isolated chain, and is essentially unchanged whether the repeats are ordered or random on the chain. The bottom graph is obtained by tracking the status of the repeat $N = 8$ within a fiber of random chains strongly interacting with each other. The effect of these interactions is to increase the SD of the distribution (while keeping the mean unchanged), which quantifies the irregularity in the repeat unfolding sequences. (*f*) SD of the unfolding probability for various N values and different fiber designs (*a–d*). The horizontal dashed line gives the threshold above which the sequence of unfolding events deviates from the mechanical hierarchy of the individual repeats. Statistics were obtained from 75 runs. See the Supporting Material for additional data.

this predominant energy barrier is passed, unfolded repeats follow the known nonlinear regime at further extensions. The cooperative breakage of the two force-bearing bonds comes from their symmetric placement in our model. Indeed, the latter ensures that they both support the same force until one of them breaks, subsequently leaving the other to break immediately under a force it cannot bear alone. This feature is essential because the β-sheet-forming FnIII modules (and similarly the titin's immunoglobulin domains) contain a single cluster of force-bearing backbone hydrogen bonds that break simultaneously for the major energy barrier to be passed. Our single repeats thus mimic well the unfolding behavior of many β-sandwich protein domains (5,8,21,27,28,34). The amplitude of the activation peak depends linearly on N and logarithmically on ν (Fig. 1 *c*). The linear dependency on N is natural, because the force is evenly shared by each of the N bonds that form the bearing cluster. Logarithmic corrections to the linear behavior caused by the assumption that molecular damping also scales with N were discussed previously (35). The logarithmic dependency on ν is a result of the Bell model and approximately conforms with experimental observations (36,37). However, it should be noted that a number of previous studies were aimed at improving or testing the microscopic foundation, suitability, and range of applicability of the Bell model (32,33,38–41).

Single chain of repeats

Because the mechanical stabilities of different FnIII repeats can vary significantly (27,28), we design our model of a linear Fn chain by connecting lined-up repeats with different mechanical stabilities, here represented by the multiplicity N of their force-bearing cluster of bonds. These bonds are color-coded according to their value of N (Fig. 1 *d*). When we extend the multirepeat, single-chain model, we observe a sequence of force peaks similar to those seen for real multidomain proteins (28,42). In particular, using the model segment shown in the inset of Fig. 1 *d*, which is composed of $n = 10$ repeats of 10 different stabilities N between $N_{\max} - n + 1 = 2$ and $N_{\max} = 11$, we can reproduce the experimental data for a native Fn mimetic chain with 10 domains. Notably, we find that the single chain can be stretched reversibly up to 800% (Fig. 1). It has been observed for single, multidomain proteins that the weakest modules break first, independently of their position within a single chain. We thus also randomized the relative positions of mechanically weak (low N) and strong (high N) repeats within our single-molecule and -fiber simulations. We find that for both cases—ordered (i.e., with the repeats arranged in order of their force-bearing strength N) and random (with the repeats randomly placed in the fiber)—the chain opens up at the weakest repeat first (smaller N), followed by the next folded weakest module, and so on. We refer to this important feature of the isolated chain as sequential unfolding, which is dictated for single molecules by the mechanical hierarchy of the repeats.

Single fiber of chains of repeats

Remarkably, nothing is known about the sequence in which repeats unfold when embedded in fibrillar assemblies. Once multidomain proteins are assembled into fibers or materials, collective phenomena resulting from lateral repeat-repeat interactions have to be considered. Moreover, no periodicity has ever been detected in the ultrastructure of Fn fibers, and the repeats do not seem to be arranged according to their mechanical stabilities. We thus asked how the ordering or randomness with respect to their positions within the fiber might affect the mechanical stability of a fiber and its refolding kinetics. To investigate all of these potential effects, we assembled single chains of repeats into multimeric fibers of m chains stacked in parallel to each other. The interchain interaction that holds the fiber together is composed of either noncryptic interactions between sites located on the surface of a repeat, which can form labile surface bonds with bearing strength N_s (or N_s clusters), or by cryptic N_c clusters of labile bonds generated from exposed cryptic sites. The latter are enabled once the corresponding repeat unfolds. For both types of interchain bonds, we use the same force law as for the intramodule structural bonds. The noncryptic surface bonds are active as long as the repeat is folded; otherwise, they are forbidden and cryptic interaction is allowed. In this way, we ensure that the fiber integrity is dominated by cryptic sites at large extensions (14). The fibers are then defined as ordered if all of the chains have their repeats ordered according to their mechanical stability, and random for an assembly of chains with disordered repeats, whereas all chains in a fiber contain the same set of repeats. Furthermore, we consider two conditions, called slip and nonslip conditions, in which neighboring chains can or cannot, respectively, slide past each other. Slip conditions ultimately allow for fiber rupture.

Under nonslip conditions, all terminal chain ends on both sides of the fibril are pulled apart from each other, as shown in Fig. 2. With increasing extension, cryptic sites become exposed and can form stabilizing interactions to neighboring molecules. In ordered fibers, the weakest repeats break first, which creates segments of entirely unfolded chains next to segments with still folded repeats (Fig. 2 *a*). In contrast, initiation sites where repeats start to unfold are randomly distributed over the whole length of the random fibers, such that regions of unfolded repeats closely coexist with regions of still folded repeats (Fig. 2, *b–d*). Because interchain and cryptic interactions enable correlated interchain behavior, we next asked whether the sequence in which the repeats unfold is solely determined by their relative mechanical stability in the fibers. An analysis of the probability of unfolding a repeat as a function of the strain $\epsilon = L/L_0 - 1$, relative to the resting length L_0, reveals that

if the cryptic and surface interchain interactions are sufficiently weak, the mechanical stability N of a repeat indeed dictates the strain at which it unfolds (Fig. 2 *f*, *open circles connected with thin lines*), similarly to the sequential unfolding of a single chain. In fibers of strongly interacting chains, the standard deviation (SD) observed in the sequence of unfolding is large enough to allow for deviations from the sequential unfolding according to the mechanical hierarchy. Most significantly, the sequence of hierarchical unfolding is even more degraded when the strength of cryptic interactions is tuned up from $N_c = 0$ to $N_c = 50$. This loss of hierarchy in the repeats' activation has in fact been implicated experimentally: the cryptic sites on modules $FnIII_7$ and $FnIII_{15}$ are exposed continuously in a fiber with increasing strain (14), and not with two bursts at two discrete strains. Yet, it was not known from the experimental literature that this behavior is enabled by the random arrangement of mechanically weak and strong repeats within Fn fibers, and scales with the number of noncryptic and cryptic interchain interactions. Our simulations further reveal that the sequential unfolding is further depreciated with increasing repeat strength, because the SD in the sequence of unfolding accumulates to the later stages, when stronger repeats open (see Supporting Material).

In a second set of fiber simulations, we enabled molecular slippage (and fiber breakage) by pulling only on the ends of an interlaced half of the chains while holding the opposite ends of the other half fixed (see snapshots in Fig. 3 *a*). Here, the fiber is thus allowed to extend not only by unfolding of its repeats but also through chain slippage. The initial events that occur for small fiber extensions are similar in principle to those described above for nonslip conditions, particularly concerning the changes with ordered or random chains and with cryptic or noncryptic interchain interactions (Figs. 2, *a–d*, and 3, *a* and *b*). However, we can also determine how these parameters regulate the fiber behavior at large extensions. The resulting stress-strain response of the fiber is shown in Fig. 3 *c* for moderate surface interchain interactions, $N_s = 15$, and various cryptic bearing strengths. This intermediate value of N_s is chosen to avoid the following two extreme scenarios. If we would have taken $N_s \ll 15$, the chains would slide against each other and most of the repeats would remain folded during the breakage of the fiber. If we would haven chosen $N_s \gg 15$, the role of the cryptic sites would be hidden. With $N_s = 15$, sliding is reduced and activated cryptic bonds are stretched. The stress σ is determined using $F = A_0\sigma$, the measured force to stretch a fiber with an effective cross-sectional area A_0. We determined this coarse-graining parameter, $A_0 = 560\text{nm}^2$, by using the experimental curve shown in Fig. 3 *c*. Note that this value of A_0 coincides with the area $(md_0)^2$ for $d_0 \approx 1.65a = 2.15$ nm, the effective diameter of a single repeat. The resulting stress-strain curves exhibit at lower strain, $\epsilon < 400\%$, a nonlinear elastic regime that is independent of the cryptic bond strength N_c. In this regime, the apparent successive force peaks reflect the chain's intrinsic behavior and the ideal boundary conditions we used. They would smooth out for realistic fibers that are made with a larger number of molecules. At further extensions, the fibers with weaker or no cryptic bonds show more slippage and are the ones that break first. Yielding occurs at higher strain for higher N_c. In particular, cryptic fibers with $N_c = 65$ exhibit a maximum strain of 800%, a value very similar to that found in real Fn fibers (14), below which the fiber remains intact. For this value of N_c, significant hardening of the material can be observed when $400\% < \epsilon < 800\%$, before yielding. This originates from the intrinsic nonlinear behavior of the extended chains (see Fig. 1 *d* at extensions $L > 270$ nm) and from the increasing number of stiff cryptic bonds at large extensions. Nonlinear strain hardening is indeed observed on actual Fn fibers under tensile tests (14), as reported here in Fig. 3 *c* (*black line*).

Refolding and misfolding of repeats, chains, and fibers

Refolding is an essential feature of most molecules, assemblies, and molecular fibers that perform mechanical functions in cells and tissues (14,43,44). Single-molecule force spectroscopy revealed that a large fraction of repeats can refold into their original secondary structure (45), and many biological fibers can readily contract to the original contour length and regain their mechanical characteristics once the tension is released (14,46–48). For our single isolated module, we see that a short-lived intermediate is formed first, followed by a transient bifurcation of refolding pathways. Proper refolding leads to the original Z-shaped repeat with two bearing bonds, and misfolding or transient misfolding results in an alternate secondary structure of the repeats that does not have force-bearing bonds (Fig. 4 *a*). We measured that 72% of the isolated repeats refold into the force-bearing state with a characteristic time of ~0.5 s (Fig. 4 *b*) within the timeframe of our simulations. Both the proper folding fraction and the rate do not depend on the bearing strength N of the repeats. When integrated into a single multirepeat chain, successful refolding appears to be slightly upregulated because nearly 78% of repeats in the chains eventually refold properly within the simulated timeframe of 6 s. The prevalence of proper folding supports our choice of model parameters, although we could not find any experimental measurements of the proportion of transiently misfolded Fn repeats. However, the cycle of mechanical unfolding and refolding of ubiquitin has been investigated in more detail using force ramps. For this system, a simple two-state model is consistent with the folding kinetics under different force-clamp conditions (43), whereas there are indications of the existence of at least transiently misfolded states (43). This picture seems consistent with our findings regarding the Fn-mimetic repeats modeled here.

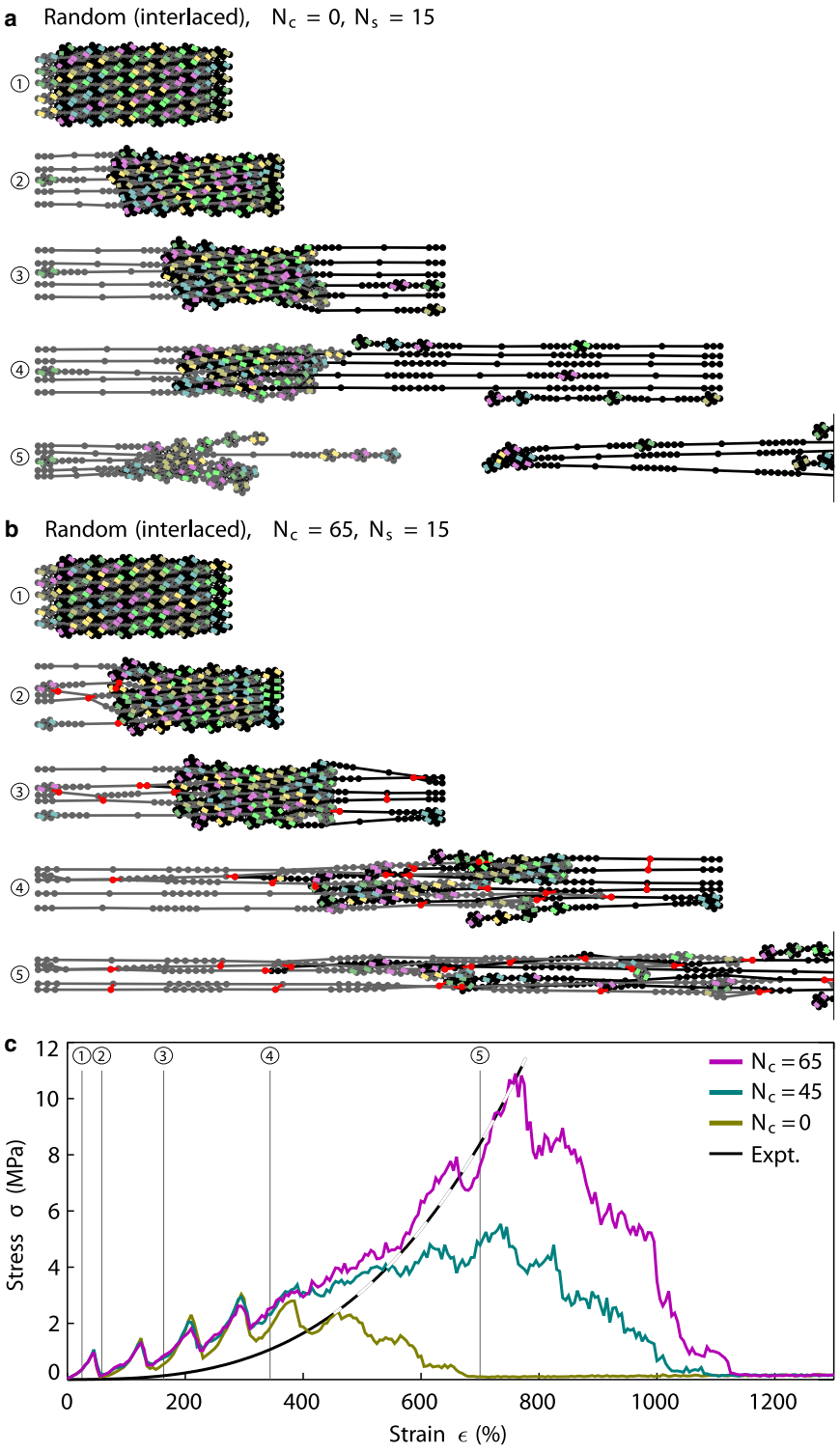

FIGURE 3 Mechanoregulated strengthening of random fibers with interlaced comb structure ($m = 11$, $n = 6$,$N_{max} = 11$, $N_s = 15$) due to cryptic sites; the results obtained for ordered fibers are not significantly different. (*a*) Snapshot of the extended fiber without cryptic sites; the fiber eventually ruptures. (*b*) Extensional test for a fiber with strong cryptic sites, $N_c = 65$ (both tests shown in Movie S2). (*c*) Corresponding stress-strain curves for various cryptic bonds' bearing strengths; the black full line is the experimental fit proposed by Klotzsch et al. (14) upon pulling of actual Fn fibers (in that work, the stress was actually measured reliably up to only $\varepsilon = 450\%$). The dotted line marks the extrapolated fit for which no experimental evidence is available; the circled numbers refer to the frame presented in panels *a* and *b* (note that the last frame of each panel is truncated on the right-hand side). Statistics were obtained from 15 runs.

Next, we study the refolding kinetics of the stretched molecular assemblies into fibrillar structures. After stretching the fibers under nonslip conditions, we observe that the majority of repeats are misfolded upon relaxation (Fig. 4 *a*). We note that when they are integrated into a fiber, the misfolded repeats perdure within the simulated timeframe, and only a vanishing small fraction of repeats eventually stay unfolded under the chosen thermodynamic conditions. Lateral crowding thus lowers the propensity of the repeats to refold properly, without preventing the complete retraction of the fibers, and the fraction of misfolded modules increases with the cryptic interchain binding strength N_c.

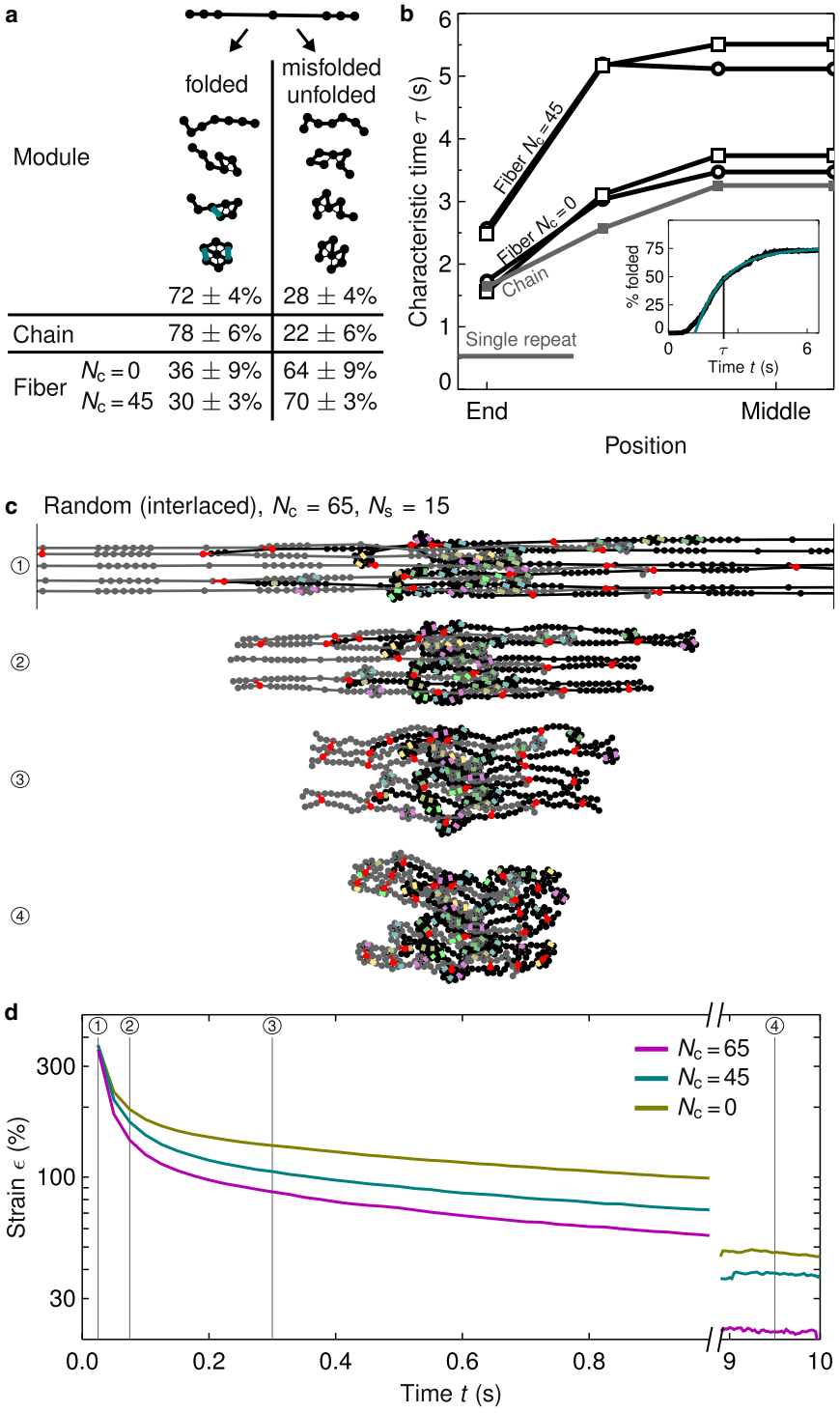

FIGURE 4 Relaxation behavior of single repeats, chains, and fibers. Unless otherwise mentioned, the fibers are initially stretched as in Fig. 2 to prevent chain sliding. (*a*) The folding pathway of a repeat can lead to a properly folded state or a misfolded state with the displayed proportions. In chains ($n = 6$) and fibers ($m = 11$, $N_s = 1$), the repeats may also misfold or not refold at all. (*b*) Characteristic time for a repeat to properly refold when isolated (*gray horizontal line*), or built in chain and fiber, as a function of its position in the assembly (*symbols* as in Fig. 3). For each position we fit the fraction of folded repeat as a function of time with a single-time exponential function, as shown in the inset; as opposed to the characteristic time, the plateau does not significantly depend on the position in the assembly, and gives the refolding statistics shown in panel *a*. (*c*) Snapshots of an interlaced fiber's relaxation after being stretched as shown in Fig. 3. (*d*) Fiber strain as a function of time corresponding to the snapshots presented in panel *c*. Statistics were obtained from 10 runs.

The refolding rate depends strongly on the position of the repeat in the chain or the fiber. Repeats at the ends refold faster than the repeats at the center (Fig. 4 *b*) because the latter can refold only when larger segments have relaxed and come together. The dynamics of refolding of single chains can be readily described by a single exponential (*inset* of Fig. 4 *b*) with time constants between 1 and 3s, in agreement with experiments (28). An exponential time course is consistent with a memory-free Markovian process in which the probability of unfolding at any given time is independent of the previous history (43). Refolding the repeats of fibers with strong cohesive cryptic bonds ($N_c = 45$) takes between 2 and 6s, and this characteristic time appears to be slightly reduced for random fibers.

Although fibrillogenesis and cryptic interactions thus increase the tensile strength of fibrillar assemblies, we also find that the fraction of transiently misfolded modules increases with cohesive forces N_c within fibrils but decreases with decreasing fiber thickness (Fig. 4). These results have a major physiological significance: Because Fn fibrils in the ECM have been reported with diameters ranging from 20 nm to a few micrometers (49–51) (i.e., 10–10^3 repeats per cross section), one would expect very different fractions of misfolding between the thin and thick fibers. Furthermore, we report for the first time, to our knowledge, that a random arrangement of mechanically strong and weak repeats within a fiber can reduce their characteristic refolding times (Fig. 4).

For comparison with available experiments, we studied the relaxation kinetics of fibers initially stretched to $\epsilon = 400\%$. The strain-relaxation exhibits two different kinetic regimes: at short times, the stretched permanent bonds relax first, followed by the slow repeats' refolding and the reorganization of secondary structures. Such relaxation kinetics were also observed experimentally on Fn fibers (14). For fibers with a moderate number of cryptic interactions (here $N_c \leq 45$), plastic deformations resulting from the chains sliding during the initial stretch prevent the fibers from recovering their initial length. Indeed, the preconditioning strain of 400% is the typical onset of yielding for fibers with weak cryptic bonds, as shown in Fig. 3 *c*. For the same value of strain, experiments show that the fiber recovers a length only 10% longer than its rest length after ~10 s (14). Our model yields similar times for $N_c = 65$, although the simulations do not allow us to wait minutes for the full relaxation of the fiber to its initial rest length. We note that the relaxed fiber in Fig. 4 *c* has a significant population of cryptic bonds. In a subsequent stretching experiment (results not shown), these preexisting bonds did not alter the nonlinear hardening of the stress-strain curve that arose from extending the cryptic bonds, irrespective of their prior state.

CONCLUSIONS

Guided by the design of Fn, we developed a coarse-grained model for fibers assembled from chains of repeats, each of which consists of a mechanochemical switch. We parametrized our model using existing experiments at the single-chain level (Fig. 1). With this parameter set, we were able to correctly predict central physical features that were independently and experimentally reported for the fibrillar assemblies (Figs. 3 and 4). Consequently, this model allows us to explore questions about how the design of Fn relates to the fiber characteristics (Fig. 2)—questions that are still difficult to address experimentally.

Using our model, we found that both yielding and breakage of Fn fibers are strongly retarded by the presence of cryptic sites that strengthen lateral interchain interactions upon stretching (Fig. 3). We found that the cryptic sites are indeed responsible for the nonlinearity in the stress-strain curve of the fibers, from soft to strain-hardened (Fig. 3). Various cryptic sites may be involved in Fn fibrillogenesis (52,53): 1), Fn has cryptic cysteines that can be exposed by the unfolding of the $FnIII_7$ and $FnIII_{15}$ modules; 2), single β-strands may bind and thereby extend the β-sheets of the FnI and FnIII repeats (52,54); and 3), module unfolding can expose hydrophobic residues that may also act as cryptic sites (52). Furthermore, our fiber model predicts for the first time, to our knowledge, that the breakage of repeats does not follow the mechanical hierarchy of their activation barriers when the forces that ensure the fiber's cohesion, such as surface (N_s) and cryptic (N_c) interactions, are strong (Fig. 2). Gaining insights into the conservation or loss of the repeats' mechanical hierarchy in chains and fibers has major implications for the functional properties of such assemblies. For Fn and many other multidomain proteins, the repeats often carry molecular recognition sites for different partners (7). Deciphering the sequence by which the repeats are unfolded and activated (or inactivated) will help us understand how multimodular extra- or intracellular proteins can be exploited by cells as mechanochemical signal transducers to sense a large range of mechanical strains, and determine whether some recognition sites are activated or destroyed at a specific strain or are more gradually affected by the strain.

The design principles described in this work can be generalized to create both strong and tough polymeric materials, a significant goal in the materials science community. Previous investigators synthesized polymer coils (2,15,55–57) and foldamers (58) that resemble the globular structure modeled here, and these units were subsequently cross-linked into extensive networks (2,15,55–57). Much as in our system, the intramolecular bonds (i.e., those within the folded structures) were weak, labile bonds, and the intermolecular bonds were taken to be strong bonds. Such biomimetic systems were shown to exhibit useful mechanical properties (2,15,55–57). Our findings provide useful guidelines for optimizing the mechanical performance of such synthetic, biomimetic systems.

Our model can be extended to describe other multidomain extra- and intracellular proteins and their assemblies. For example, one could represent the Ig domains of titin, which form mechanically more stable β-sandwich motifs (59), by choosing higher N values for labile bonds, thereby reflecting the higher energy barrier that has to be overcome to destroy their secondary structure. By deriving minimalistic models that capture the essence of biological mechanochemical signal converters, we can define the crucial functional units and thus help chemists and synthetic biologists to engineer de novo molecules whose functions are switched by mechanical forces. This exciting field, which shows great promise in the biomedical and engineering context, is still in its infancy.

SUPPORTING MATERIAL

Supporting equations, figures, references, and table are available at http://www.biophysj.org/biophysj/supplemental/S0006-3495(12)01069-7.

O.P., T.S., V.V., and M.K. designed the research; the topic was inspired by discussions among O.P., V.V., and A.B.; O.P. performed the simulations; O.P., T.S., and M.K. analyzed the data; O.P., M.K., I.S., and G.K. developed the model and code, adapted from previous work by G.K., I.S., and A.B.; and T.S., V.V., M.K., and O.P. wrote the paper.

This work was supported by the grants from the Swiss National Science Foundation (SNF-310030B_133122 to V.V. and SNF-SCOPES IZ73Z0_128169 to M.K.) and the European Research Council (ERC-2009-advanced grant 233157 to V.V.). All computational simulations were conducted at the ETH Brutus cluster. I.G.S. received partial support from the U.S. Department of Energy, and G.V.K. received partial support from the Army Research Office.

REFERENCES

1. Davis, D. A., A. Hamilton, …, N. R. Sottos. 2009. Force-induced activation of covalent bonds in mechanoresponsive polymeric materials. *Nature.* 459:68–72.
2. Kushner, A. M., J. D. Vossler, …, Z. Guan. 2009. A biomimetic modular polymer with tough and adaptive properties. *J. Am. Chem. Soc.* 131:8766–8768.
3. Mertz, D., C. Vogt, …, P. Lavalle. 2009. Mechanotransductive surfaces for reversible biocatalysis activation. *Nat. Mater.* 8:731–735.
4. Zhang, J., X. Lu, …, Y. Han. 2005. Reversible superhydrophobicity to superhydrophilicity transition by extending and unloading an elastic polyamide film. *Macromol. Rapid Commun.* 26:477–480.
5. Lv, S., D. M. Dudek, …, H. Li. 2010. Designed biomaterials to mimic the mechanical properties of muscles. *Nature.* 465:69–73.
6. Pearlstein, E., L. I. Gold, and A. Garcia-Pardo. 1980. Fibronectin: a review of its structure and biological activity. *Mol. Cell. Biochem.* 29:103–128.
7. Vogel, V. 2006. Mechanotransduction involving multimodular proteins: converting force into biochemical signals. *Annu. Rev. Biophys. Biomol. Struct.* 35:459–488.
8. Vogel, V., and M. Sheetz. 2006. Local force and geometry sensing regulate cell functions. *Nat. Rev. Mol. Cell Biol.* 7:265–275.
9. Sawada, Y., M. Tamada, …, M. P. Sheetz. 2006. Force sensing by mechanical extension of the Src family kinase substrate p130Cas. *Cell.* 127:1015–1026.
10. Little, W. C., R. Schwartlander, …, V. Vogel. 2009. Stretched extracellular matrix proteins turn fouling and are functionally rescued by the chaperones albumin and casein. *Nano Lett.* 9:4158–4167.
11. del Rio, A., R. Perez-Jimenez, …, M. P. Sheetz. 2009. Stretching single talin rod molecules activates vinculin binding. *Science.* 323:638–641.
12. Hytönen, V. P., and V. Vogel. 2008. How force might activate talin's vinculin binding sites: SMD reveals a structural mechanism. *PLOS Comput. Biol.* 4:e24.
13. Johnson, C. P., H.-Y. Tang, …, D. E. Discher. 2007. Forced unfolding of proteins within cells. *Science.* 317:663–666.
14. Klotzsch, E., M. L. Smith, …, V. Vogel. 2009. Fibronectin forms the most extensible biological fibers displaying switchable force-exposed cryptic binding sites. *Proc. Natl. Acad. Sci. USA.* 106:18267–18272.
15. Kushner, A. M., V. Gabuchian, …, Z. Guan. 2007. Biomimetic design of reversibly unfolding cross-linker to enhance mechanical properties of 3D network polymers. *J. Am. Chem. Soc.* 129:14110–14111.
16. Adhikari, A. S., J. Chai, and A. R. Dunn. 2011. Mechanical load induces a 100-fold increase in the rate of collagen proteolysis by MMP-1. *J. Am. Chem. Soc.* 133:1686–1689.
17. Puchner, E. M., A. Alexandrovich, …, M. Gautel. 2008. Mechanoenzymatics of titin kinase. *Proc. Natl. Acad. Sci. USA.* 105:13385–13390.
18. Chabria, M., S. Hertig, …, V. Vogel. 2010. Stretching fibronectin fibres disrupts binding of bacterial adhesins by physically destroying an epitope. *Nat. Commun.* 1:135.
19. Hynes, R. O. 2009. The extracellular matrix: not just pretty fibrils. *Science.* 326:1216–1219.
20. Gao, M., D. Craig, …, K. Schulten. 2003. Structure and functional significance of mechanically unfolded fibronectin type III1 intermediates. *Proc. Natl. Acad. Sci. USA.* 100:14784–14789.
21. Lu, H., B. Isralewitz, …, K. Schulten. 1998. Unfolding of titin immunoglobulin domains by steered molecular dynamics simulation. *Biophys. J.* 75:662–671.
22. Sotomayor, M., and K. Schulten. 2007. Single-molecule experiments in vitro and in silico. *Science.* 316:1144–1148.
23. Erickson, H. P. 1994. Reversible unfolding of fibronectin type III and immunoglobulin domains provides the structural basis for stretch and elasticity of titin and fibronectin. *Proc. Natl. Acad. Sci. USA.* 91:10114–10118.
24. Ackbarow, T., S. Keten, and M. J. Buehler. 2009. A multi-timescale strength model of alpha-helical protein domains. *J. Phys. Condens. Matter.* 21:035111.
25. Ackbarow, T., D. Sen, …, M. J. Buehler. 2009. Alpha-helical protein networks are self-protective and flaw-tolerant. *PLoS ONE.* 4:e6015.
26. Bertaud, J., Z. Qin, and M. J. Buehler. 2009. Atomistically informed mesoscale model of alpha-helical protein domains. *Int. J. Multiscale Comput. Eng.* 7:237–250.
27. Craig, D., M. Gao, …, V. Vogel. 2004. Tuning the mechanical stability of fibronectin type III modules through sequence variations. *Structure.* 12:21–30.
28. Oberhauser, A. F., C. Badilla-Fernandez, …, J. M. Fernandez. 2002. The mechanical hierarchies of fibronectin observed with single-molecule AFM. *J. Mol. Biol.* 319:433–447.
29. Salib, I. G., G. V. Kolmakov, …, A. C. Balazs. 2011. Using mesoscopic models to design strong and tough biomimetic polymer networks. *Langmuir.* 27:13796–13805.
30. Kröger, M. 2005. Models for Polymeric and Anisotropic Liquids. Springer, Berlin.
31. Warner, H. R. 1972. Kinetic theory and rheology of dilute suspensions of finitely extendible dumbbells. *Ind. Eng. Chem. Fundam.* 11:379–397.
32. Dudko, O. K., J. Mathé, …, G. Hummer. 2007. Extracting kinetics from single-molecule force spectroscopy: nanopore unzipping of DNA hairpins. *Biophys. J.* 92:4188–4195.
33. Hummer, G., and A. Szabo. 2003. Kinetics from nonequilibrium single-molecule pulling experiments. *Biophys. J.* 85:5–15.
34. Freddolino, P. L., C. B. Harrison, …, K. Schulten. 2010. Challenges in protein folding simulations: timescale, representation, and analysis. *Nat. Phys.* 6:751–758.
35. Evans, E. 2001. Probing the relation between force—lifetime—and chemistry in single molecular bonds. *Annu. Rev. Biophys. Biomol. Struct.* 30:105–128.
36. Chen, S., and T. A. Springer. 2001. Selectin receptor-ligand bonds: Formation limited by shear rate and dissociation governed by the Bell model. *Proc. Natl. Acad. Sci. USA.* 98:950–955.
37. Evans, E., and K. Ritchie. 1999. Strength of a weak bond connecting flexible polymer chains. *Biophys. J.* 76:2439–2447.
38. Dudko, O. K., G. Hummer, and A. Szabo. 2006. Intrinsic rates and activation free energies from single-molecule pulling experiments. *Phys. Rev. Lett.* 96:108101.
39. Dudko, O. K., A. E. Filippov, …, M. Urbakh. 2003. Beyond the conventional description of dynamic force spectroscopy of adhesion bonds. *Proc. Natl. Acad. Sci. USA.* 100:11378–11381.

40. Getfert, S., M. Evstigneev, and P. Reimann. 2009. Single-molecule force spectroscopy: practical limitations beyond Bell's model. *Physica A.* 388:1120–1132.

41. Husson, J., and F. Pincet. 2008. Analyzing single-bond experiments: influence of the shape of the energy landscape and universal law between the width, depth, and force spectrum of the bond. *Phys. Rev. E Stat. Nonlin. Soft Matter Phys.* 77:026108.

42. Forman, J. R., and J. Clarke. 2007. Mechanical unfolding of proteins: insights into biology, structure and folding. *Curr. Opin. Struct. Biol.* 17:58–66.

43. Schlierf, M., H. B. Li, and J. M. Fernandez. 2004. The unfolding kinetics of ubiquitin captured with single-molecule force-clamp techniques. *Proc. Natl. Acad. Sci. USA.* 101:7299–7304.

44. Vogel, V., and M. P. Sheetz. 2009. Cell fate regulation by coupling mechanical cycles to biochemical signaling pathways. *Curr. Opin. Cell Biol.* 21:38–46.

45. Ainavarapu, S. R. K., J. Brujic, …, J. M. Fernandez. 2007. Contour length and refolding rate of a small protein controlled by engineered disulfide bonds. *Biophys. J.* 92:225–233.

46. Gautieri, A., S. Vesentini, …, M. J. Buehler. 2012. Viscoelastic properties of model segments of collagen molecules. *Matrix Biol.* 31:141–149.

47. Liu, W., C. R. Carlisle, …, M. Guthold. 2010. The mechanical properties of single fibrin fibers. *J. Thromb. Haemost.* 8:1030–1036.

48. Puxkandl, R., I. Zizak, …, P. Fratzl. 2002. Viscoelastic properties of collagen: synchrotron radiation investigations and structural model. *Philos. Trans. R. Soc. Lond. B Biol. Sci.* 357:191–197.

49. Chen, L. B., A. Murray, …, M. L. Walsh. 1978. Studies on intercellular LETS glycoprotein matrices. *Cell.* 14:377–391.

50. Peters, D. M. P., Y. Chen, …, S. Brummel. 1998. Conformation of fibronectin fibrils varies: discrete globular domains of type III repeats detected. *Microsc. Microanal.* 4:385–396.

51. Singer, I. I. 1979. The fibronexus: a transmembrane association of fibronectin-containing fibers and bundles of 5 nm microfilaments in hamster and human fibroblasts. *Cell.* 16:675–685.

52. Bultmann, H., A. J. Santas, and D. M. P. Peters. 1998. Fibronectin fibrillogenesis involves the heparin II binding domain of fibronectin. *J. Biol. Chem.* 273:2601–2609.

53. Gee, E. P. S., D. E. Ingber, and C. M. Stultz. 2008. Fibronectin unfolding revisited: modeling cell traction-mediated unfolding of the tenth type-III repeat. *PLoS ONE.* 3:e2373.

54. Litvinovich, S. V., S. A. Brew, …, K. C. Ingham. 1998. Formation of amyloid-like fibrils by self-association of a partially unfolded fibronectin type III module. *J. Mol. Biol.* 280:245–258.

55. Guan, Z. 2007. Supramolecular design in biopolymers and biomimetic polymers for advanced mechanical properties. *Polym. Int.* 56:467–473.

56. Shi, Z.-M., J. Huang, …, Z. Guan. 2010. Foldamers as cross-links for tuning the dynamic mechanical property of methacrylate copolymers. *Macromolecules.* 43:6185–6192.

57. Yu, T. B., Z. Bai, and Z. Guan. 2009. Cycloaddition-promoted self-assembly of a polymer into well-defined beta-sheet and hierarchical nanofibrils. *Angew. Chem. Int. Ed.* 48:1097–1101.

58. Hill, D. J., M. J. Mio, …, J. S. Moore. 2001. A field guide to foldamers. *Chem. Rev.* 101:3893–4012.

59. Marszalek, P. E., H. Lu, …, J. M. Fernandez. 1999. Mechanical unfolding intermediates in titin modules. *Nature.* 402:100–103.

60. Craig, D., A. Krammer, …, V. Vogel. 2001. Comparison of the early stages of forced unfolding for fibronectin type III modules. *Proc. Natl. Acad. Sci. USA.* 98:5590–5595.